Hindawi
Advances in Materials Science and Engineering
Volume 2018, Article ID 6457534, 10 pages
https://doi.org/10.1155/2018/6457534

*Research Article*

# Study of Structure and Magnetic Properties of $SmCo_{10}$ Alloy Prepared by Different Methods

**Xiang Chi,[1] Ying Li,[1] De-quan Er,[2] Xu-hao Han,[1] Xiu-li Duan,[1] Ji-bing Sun,[1] and Chun-xiang Cui[1]**

[1]*Key Laboratory for New Type of Functional Materials in Hebei Province, Hebei University of Technology, No. 1 Dingzigu Road, Hongqiao District, Tianjin 300130, China*
[2]*University of Pennsylvania, 3231 Walnut Street, Philadelphia, PA 19104, USA*

Correspondence should be addressed to Ji-bing Sun; hbgdsjb@126.com

Received 11 November 2017; Revised 7 January 2018; Accepted 7 February 2018; Published 29 March 2018

Academic Editor: Peter Majewski



In this paper, the phase compositions, microstructures, atomic structures, and magnetic properties of Co-rich $SmCo_{10}$ alloys prepared by arc-melting, annealing, and melt-spinning were studied. It was found that as-cast alloy is composed of $Th_2Zn_{17}$-type $Sm_2Co_{17}$ matrix with an average grain size of ~45 $\mu$m accompanied by lamellar eutecticum (consisting of α-Co and $Th_2Zn_{17}$-type $Sm_2Co_{17}$) distributed at grain boundaries. The annealed alloy has the same phase composition and phase distribution as the as-cast alloy except that the average grain size decreases to ~35 $\mu$m, and the eutecticum has more homogeneous distribution on the matrix. Simultaneously, the atomic structure of $Sm_2Co_{17}$ is unchanged with only a decrease in structural disorder after annealing. The as-spun ribbons are composed of ~95.5 vol.% $TbCu_7$-type $Sm_2Co_{17}$ and the rest α-Co. The short rod-shaped α-Co grains are intermittently distributed at the grain boundaries of equiaxed $Sm_2Co_{17}$ grains. The as-spun ribbons show a higher coercivity, and the annealed alloy shows maximum magnetization. The structural parameters were calculated by Extended X-ray Absorption Fine Structure (EXAFS), and the relationship between structure and magnetic properties was discussed in detail.

## 1. Introduction

Sm-Co magnetic materials have been applied in various areas due to their excellent magnetic properties, especially in high-temperature field [1]. The Curie temperature ($T_c$) of the Sm-Co phase improves with increasing Co concentration. For example, the $T_c$ of $SmCo_2$, $SmCo_3$, $Sm_2Co_7$, $Sm_5Co_{19}$, $SmCo_5$, and $Sm_2Co_{17}$ are 226.7 K, 590 K, 713 K, 830 K, 1020 K, 1195 K, respectively [2], indicating that the $Sm_2Co_{17}$ alloy possesses more excellent magnetic thermal stability. However, the pure binary $Sm_2Co_{17}$ alloy has poor magnetic properties. Song et al. [3] have reported that the $Sm_2Co_{17}$ alloy prepared by induction melting shows a rhombohedral $Th_2Zn_{17}$-type $Sm_2Co_{17}$ (2:17R, for short) structure, and the as-quenched $Sm_2Co_{17}$ alloy has a hexagonal $TbCu_7$-type $Sm_2Co_{17}$ (1:7H, for short) structure. The $Sm_2Co_{17}$ alloy with 2:17R or 1:7H structure almost has no coercivity and remanence. However, they found that when the $Sm_2Co_{17}$ alloy was prepared by high-energy ball milling followed by spark plasma sintering (SPS), it consisted of hexagonal $Th_2Ni_{17}$-type $Sm_2Co_{17}$ (2:17H) structure, whose coercivity and remanence reached 4.19 kOe and 5.81 kGs, respectively. As is well known, $Sm(Co,Fe,Cu,Zr)_z$ magnets have large anisotropy fields and high Curie temperatures, which make them ideal candidates for applying in high-temperature environments. However, the high coercivity in these magnets depends on a complex heat treatment consisting of homogenization at high temperatures (1100–1200°C) followed by aging treatment for several hours at the temperature range of 800–850°C and slow cooling to 400°C [4]. References [5–9] give that the cellular microstructure, consisting of rhombohedral $Sm_2(Co,Fe)_{17}$ cells surrounded by a Cu-rich hexagonal $Sm(Co,Cu)_5$ cell boundary phase, superimposed on a coherent and thin Zr-rich lamellar phase parallel to *c*-axis, is formed after the complex heat treatment process. Among them, the $Sm_2(Co,Fe)_{17}$ cells are responsible for the saturation

magnetization, while the $Sm(Co,Cu)_5$ at cell boundaries pins the domain walls. Additionally, the existence of the Zr-rich lamellar phase promotes the segregation of Cu in cell boundaries by providing easy diffusion paths, which results in a significant difference in domain wall energy between $Sm_2(Co,Fe)_{17}$ and $Sm(Co,Cu)_5$, improving the domain wall pinning effect. Durst et al. [6] reported that, by homogenizing at 1160°C and subsequent aging at 840°C for 24 h followed by a slow cooling to 400°C in 3 h, the $Sm(Co,Fe,Cu,Zr)_{7.6}$ magnet attains a coercivity of 35 kOe. However, the coercivity of the magnet decreases to only 0.2 kOe when the process of slow cooling is omitted. The similar phenomenon is also reported by Gutfleisch et al. [10], who found that the coercivity of $Sm(Co_{0.784}Fe_{0.100}Cu_{0.088}Zr_{0.028})_{7.19}$ magnet reached ~30 kOe when slow cooling (0.7 K/min) from the aging temperature of 850°C was adopted. However, when the magnet was quenched from the aging temperature, its coercivity reduced to less than 1 kOe due to the coarsening of domains in 2:17R cells. The change of domain structure is attributed to the change of Cu content in the 1 : 5 cell boundary phase, resulting in change of the exchange coupling between 2:17R cells.

Chen et al. [11] found that the coercivity of $SmCo_x$ ($x = 8.5$–$10.0$) having a $Sm_2Co_{17}$/Co microstructure prepared by ball milling and subsequent annealing is close to some grades of $Sm_2TM_{17}$ (TM = Co, Fe, Cu, and Zr) magnets although the $SmCo_x$ alloys contain no precipitation hardening elements, such as Cu and Zr. Among them, the $SmCo_{10}$ alloy has the highest coercivity of 4.0 kOe. They explained the coercivity mechanism of the $Sm_2Co_{17}$/Co system by domain wall pinning effect resulting from the cobalt precipitate or the grain boundaries of the $Sm_2Co_{17}$ phase.

It seems that the Co-rich Sm-Co alloys with $Sm_2Co_{17}$/Co two-phase microstructures have potentially good hard magnetic properties. However, there are few reports on this kind of alloy. In this paper, we comparatively studied the microstructures and magnetic properties of $SmCo_{10}$ alloys at as-cast, annealed, and as-spun states. In addition, we report an Extended X-ray Absorption Fine Structure (EXAFS) method to analyze their atomic structures, which has not been reported before.

## 2. Materials and Methods

The Co-rich alloy with a nominal composition of $SmCo_{10}$ was prepared using pure Sm and Co, while extra 10 wt% Sm was added to compensate for the vaporization of Sm during melting. The parent alloy was arc-melted four times and cooled to room temperature (RT) by water-cooled copper crucible to obtain the as-cast bulk alloy (for short as-cast alloy). Then parts of as-cast alloy was annealed at 820°C for 120 min to obtain the annealed bulk alloy (for short annealed alloy), while the rest was melt-spun at a roller speed of 40 m/s to obtain as-spun ribbons.

Three $SmCo_{10}$ alloys were ground into powders in ethanol. The phase compositions of samples were analyzed by Rigaku $D_{max}$ 2500 PC X-ray diffractometer (XRD) with Cu $K_\alpha$ radiation and a graphite monochromator. The phase morphology and composition distribution were observed by FEI Inspect S50 scanning electron microscope (SEM) with Everhardt-Thornley Second Electron Detector. TECNAI $G^2$ F20 transmission electron microscopy (TEM) was used to observe the microstructure of as-spun ribbons. Ribbon specimens for TEM observation were prepared by ion milling. The measurements of magnetic properties were carried out on LakeShore 7407 vibrating sample magnetometer (VSM) with a maximum field of 20 kOe. To obtain ideal coercivity performances, all samples were magnetized in a 50 kOe pulsed magnetic field before VSM measurement. The as-cast and as-annealed alloys were prepared to bond magnets before measuring the hysteresis loops, while the ribbons were directly tested with the magnetization direction parallel and vertical to the external field direction, respectively. The EXAFS experiments were performed at the 4B9A beamline of the Beijing Synchrotron Radiation Facility (BSRF). The storage ring runs at 2.5 GeV with a maximum electron current of about 250 mA. The energy range of the incident X-ray is tunable from 4 to 25 keV by fix-exit Si (111) double crystal monochromator. The absorption edge of standard metal foils is used to calibrate the X-ray energy. Samples were ground into fine powers and then smeared on Scotch tapes. Sm $L_3$-edge (6716 eV) EXAFS spectra were collected at energy range from 6516 eV to 7616 eV at RT in transmission mode using ionization chamber.

## 3. Results and Discussion

*3.1. Phase Analysis.* Figure 1 shows the XRD patterns of $SmCo_{10}$ powders at different states. It suggests that as-cast and annealed alloys are composed of the $Th_2Zn_{17}$-type $Sm_2Co_{17}$ phase (for short 2:17R) with space group (S.G.) of $R\bar{3}m$, and a little pure α-Co (face-centered cubic (fcc) structure, S.G. Fm3m). The as-spun ribbons are composed of the $TbCu_7$-type $Sm_2Co_{17}$ phase (for short 1:7H) with S.G. of P6/mmm and a little pure α-Co. However, the more detailed differences in the atomic structure of $SmCo_{10}$ alloys at different states cannot be analyzed by XRD.

In fact, the $Sm_2Co_{17}$ phase can exist in $Th_2Ni_{17}$-, $TbCu_7$-, or $Th_2Zn_{17}$-type structure. There are four types of powder diffraction files (PDF) of the $Sm_2Co_{17}$ phase, whose numbers are 351368, 260484, 657762, and 190359, respectively. The $Sm_2Co_{17}$ with number 351368 belongs to the $Th_2Ni_{17}$-type $Sm_2Co_{17}$ phase (for short 2:17H) with S.G. of $P6_3/mmc$ (194) and the lattice constants are $a = 0.8373$ nm, $c = 0.8165$ nm, and $c/a = 0.9752$. The 2:17H is very unstable at RT, and only the single $Sm_2Co_{17}$ phase alloy with very fine grains (~15 nm) has the stable 2:17H structure at RT. The main reason for this is that the Gibbs free energy of 2:17H is lower than that of 2:17R when its grain size reduces to a specific value [3]. Therefore, the nonexistence of the 2:17H phase at three states of $SmCo_{10}$ alloys may be attributed to the coarse $Sm_2Co_{17}$ grains. Moreover, the PDF with number 190359 illustrates that Sm-Co alloys with 87.5–89.4 at% Co show a 2:17R structure with the lattice constants of $a = 0.8402$ nm, $c = 1.2172$ nm, and $c/a = 1.4487$ after homogeneously annealed at about 900°C, that is to say, the 2:17R phase is stable at RT. On the other hand, the other two $Sm_2Co_{17}$ with number 260484 and number 657762 belong to the 1:7H structure,

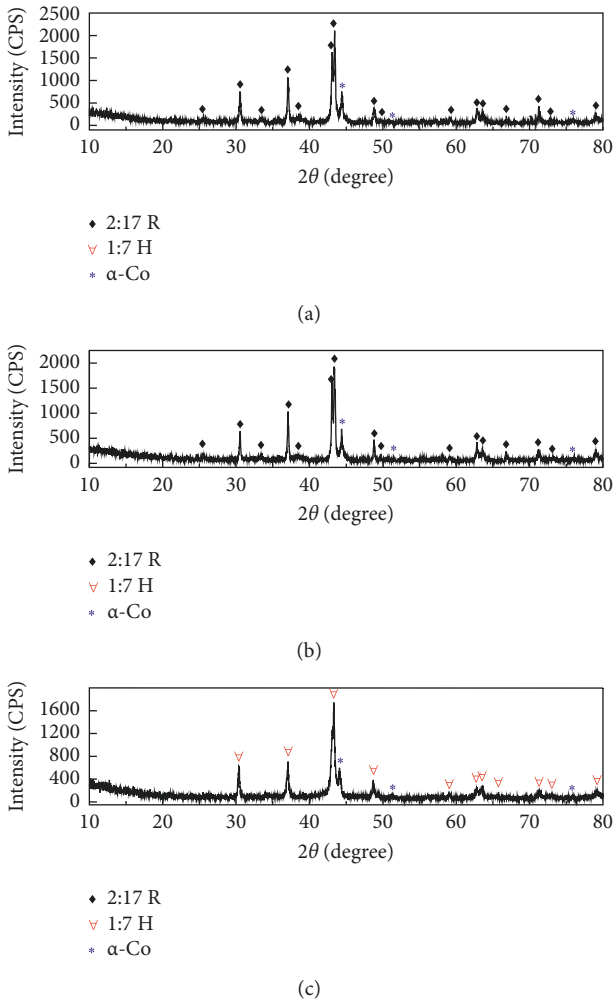


FIGURE 1: XRD patterns of $SmCo_{10}$ alloys at different states. (a) As-cast alloy. (b) Annealed alloy. (c) As-spun ribbons.

which both have the same lattice constants ($a = 0.4856$ nm, $c = 0.4081$ nm, and $c/a = 0.8404$). The PDF with number 260484 indicates that the 1:7H phase can only exist above 1320°C. At the same time, the sample in PDF with number 657762 was melted in vacuum arc furnace, followed by annealing at 1320°C for 2 h and then being cooled in liquid nitrogen. Both PDFs declare that the $Sm_2Co_{17}$ with 1:7H structure is a high-temperature phase, and the rapid cooling can inhibit the transformation from 1:7H to 2:17R. So the extremely fast cooling in melt-spinning process impedes the 1:7H→2:17R transformation and results in the 1:7H phase retained in as-spun ribbons. However, the as-cast $SmCo_{10}$ alloy was cooled by water-cooled copper crucible, whose cooling capacity is far less than that of liquid nitrogen, so the as-cast alloy is composed of 2:17R and α-Co. Since the annealing temperature is below 1320°C and the cooling rate is very low, no phase change occurs, but the microstructure of the as-cast alloy is homogenized during annealing process. Although the allotropic transformation of α-Co→ε-Co (close-packed hexagonal (hcp), S.G. $P6_3/mmc$) can occur at about 420°C, α-Co precipitated in grain boundaries may refuse the allotrope transformation. Therefore, the annealed $SmCo_{10}$ alloy is still composed of 2:17R and α-Co. Moreover, by comparing Figures 1(a)–1(c), the diffraction intensity of the as-spun ribbons is significantly lower than that of as-cast and annealed alloys, meaning that the atomic structure in as-spun ribbons has a higher disorder.

Figures 1(a) and 1(b) show that the maximum peak intensities of 2:17R and α-Co phases in as-cast alloy are 2107 CPS and 753 CPS, while those in annealed alloy are 1926 CPS and 688 CPS, respectively. Therefore, the mass fractions of 2:17R and α-Co phases in as-cast and annealed alloys are equal due to the almost equal ratios of 2107/753 (2.798) and 1926/688 (2.799). Furthermore, the actual lattice parameters of 2:17R in as-cast ($a = 0.83954$ nm, $c = 1.22374$ nm, $c/a = 1.4576$, and $V$ (cell volume) $= 0.7469\ nm^3$) and annealed ($a = 0.83947$ nm, $c = 1.22361$ nm, $c/a = 1.4576$, and $V = 0.7467\ nm^3$) alloys are obtained by XRD refinement using Jade software, which are almost the same. The $V$ of 2:17R is 0.3763% larger than that of standard 2:17R ($a = 0.8402$ nm, $c = 1.2172$ nm, $c/a = 1.4487$, and $V = 0.7441\ nm^3$). These results indicate that a small amount of Co is excessively dissolved in 2:17R and hence results in a lattice expansion, and the content of over-dissolved Co is almost unchanged after annealing. However, Figure 1(c) shows that the mass fraction of the α-Co phase in as-spun ribbons is smaller due to the larger ratio of the maximum peak intensity of 1:7H to α-Co (1743 CPS/600 CPS = 2.905). And the refinement result for lattice parameters of 1:7H ($a = 0.48605$ nm, $c = 0.41083$ nm, $c/a = 0.8452$, and $V = 0.0841\ nm^3$) shows that its $V$ is 0.9604% larger than the standard one ($a = 0.4856$ nm, $c = 0.4081$ nm, $c/a = 0.8404$, and $V = 0.0833$). It means that more Co is dissolved excessively in 1:7H than 2:17R due to the larger lattice expansion rate (0.9604%). Simultaneously, the smaller content of the α-Co phase in as-spun ribbons also confirms that 1:7H contains more supersaturated solid solution of Co than 2:17R in as-cast and annealed alloys.

*3.2. Microstructure Analysis.* Figure 2 shows the SEM images of $SmCo_{10}$ alloys in different states. It can be seen from Figure 2(a) that as-cast alloy consists of the gray matrix phase with an average grain size of ~45 $\mu$m and the bright lamellar phase discontinuously distributed on the matrix. According to the Sm-Co phase diagram [12], when liquid $SmCo_{10}$ alloy with 90.9 at% Co is cooled, the proeutectic 1:7H phase precipitates first from the liquid; subsequently, the residual liquid transforms to the lamellar eutecticum with 1:7H/α-Co atomic ratio of about 8/3 (mass ratio is ~3.47) through the eutectic reaction at 1325°C. As the temperature decreases, the transformation from 1:7H to 2:17R occurs at about 1300°C, while Co allotropic transformation does not occur. Figures 2(d) and 2(e) show the energy spectra of regions 1 and 2, which correspond to the matrix and lamellar phases, respectively, in Figure 2(a). It suggests that the lamellar areas in Figure 2(a) correspond to the eutecticum 2:17R + α-Co, where the bright particles are α-Co, and the rest of the gray part is 2:17R, same as the matrix phase. XRD analysis has given that the contents of the 2:17R and α-Co phases in as-cast and annealed alloys are almost same and the supersaturated Co in 2:17R is few. Therefore, the atomic percentages of the 2:17R and Co

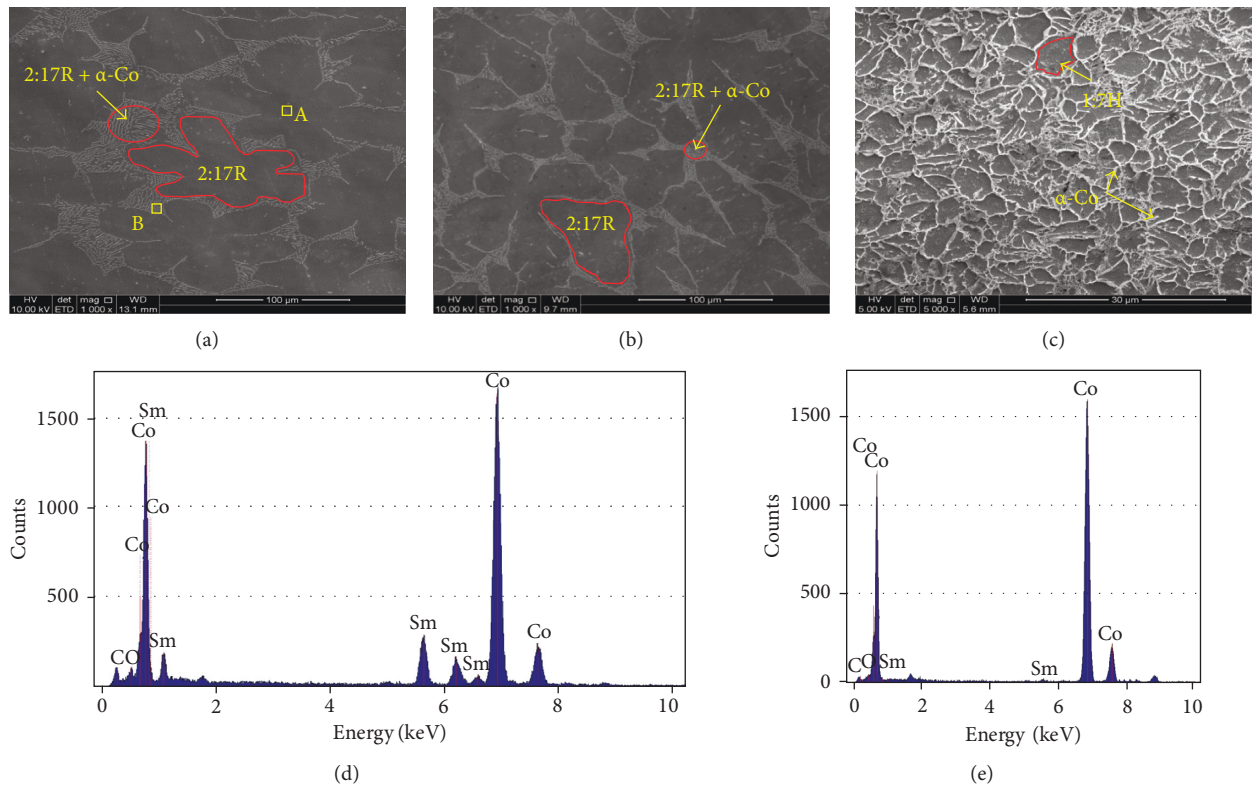


FIGURE 2: SEM images of $SmCo_{10}$ alloys. (a) As-cast alloy. (b) Annealed alloy. (c) As-spun ribbons. (d) Energy spectrum of region A in (a). (e) Energy spectrum of region B in (a).

phases in as-cast and annealed $SmCo_{10}$ alloys can be calculated to be ~86.7 at% and ~13.3 at% (mass percentages are ~89.4 wt% and ~10.6 wt%), respectively, according to the Sm-Co phase diagram [12].

Comparing Figure 2(b) with Figure 2(a), we see that, in annealed alloy, the microstructure morphology is almost the same, except that the average grain size of 2:17R decreases to ~35 $\mu$m, compared with the as-cast one. The decrease in the average size of 2:17R grains is due to the more homogeneous distribution of eutecticum 2:17R + α-Co caused by annealing. In contrast, a dramatical change occurs in the microstructure of as-spun ribbons, as shown in Figure 2(c), where the continuous grid-like bright stripes and the gray grains may be α-Co and 1:7H phases, respectively.

In order to further determine the phase composition, phase distribution and crystallization process of the as-spun ribbons, Figure 3, shows the TEM images of as-spun ribbons. It can be seen that $SmCo_{10}$ ribbons consist of approximately equiaxed grains with an average size of ~1 $\mu$m and the short rod-shaped secondary phase with the average length and width of ~400 nm and ~100 nm distributed intermittently at grain boundaries, which is different from the continuous grid-like bright morphology in Figure 2(c).

Figure 3(b) is a magnification of the region A in Figure 3(a), and the high resolution images of Figures 3(c) and 3(d) correspond to regions B and C in Figure 3(b), respectively. The results of fast Fourier transform (FFT) show that both the left (L) and right (R) regions in Figures 3(c) and 3(d) correspond to the 1:7H phase, and there is no extra grain boundary phase. Additionally, the energy spectra corresponding to Positions 1 and 2 in Figure 3(b) are presented in Figures 3(e) and 3(f), respectively. They demonstrate that the intermittent boundary phase at Position 1 and equiaxed grain at Position 2 are α-Co and 1:7H phases, respectively. Therefore, the grid-like bright stripes in Figure 2(c) are not a continuous α-Co, but consist of grain boundaries and the intermittent α-Co phase. Additionally, from the numbers and the average sizes of 1:7H and α-Co grains in Figure 3(a), we estimate their volume percentages as ~95.5% and ~4.5%, respectively. Combined with their densities (1:7H: 8.564 g/cm, α-Co: 8.788 g/cm) in PDF with number 657762 and number 150806, the mass percentages of 1:7H and α-Co are calculated to be ~95.4% and ~4.6%, respectively. Therefore, the content of α-Co is reduced after melt-spinning, which is consistent with the result of XRD analysis.

We can see from SEM and TEM images that the as-cast, annealed, and as-spun $SmCo_{10}$ alloys all form $Sm_2Co_{17}$/Co two-phase microstructure, same as that of mechanically alloyed $SmCo_{10}$ [11]. Moreover, the melt-spinning inhibits the eutectic transformation of liquid phase and impedes the 1:7H→2:17R transformation, resulting in the metastable 1:7H phase retained in as-spun ribbons.

*3.3. EXAFS Analysis.* As we know, the Rietveld refinement of XRD pattern put forward by Rietveld [13] can be used to analyze the crystal structure. In fact, XRD refinement gives

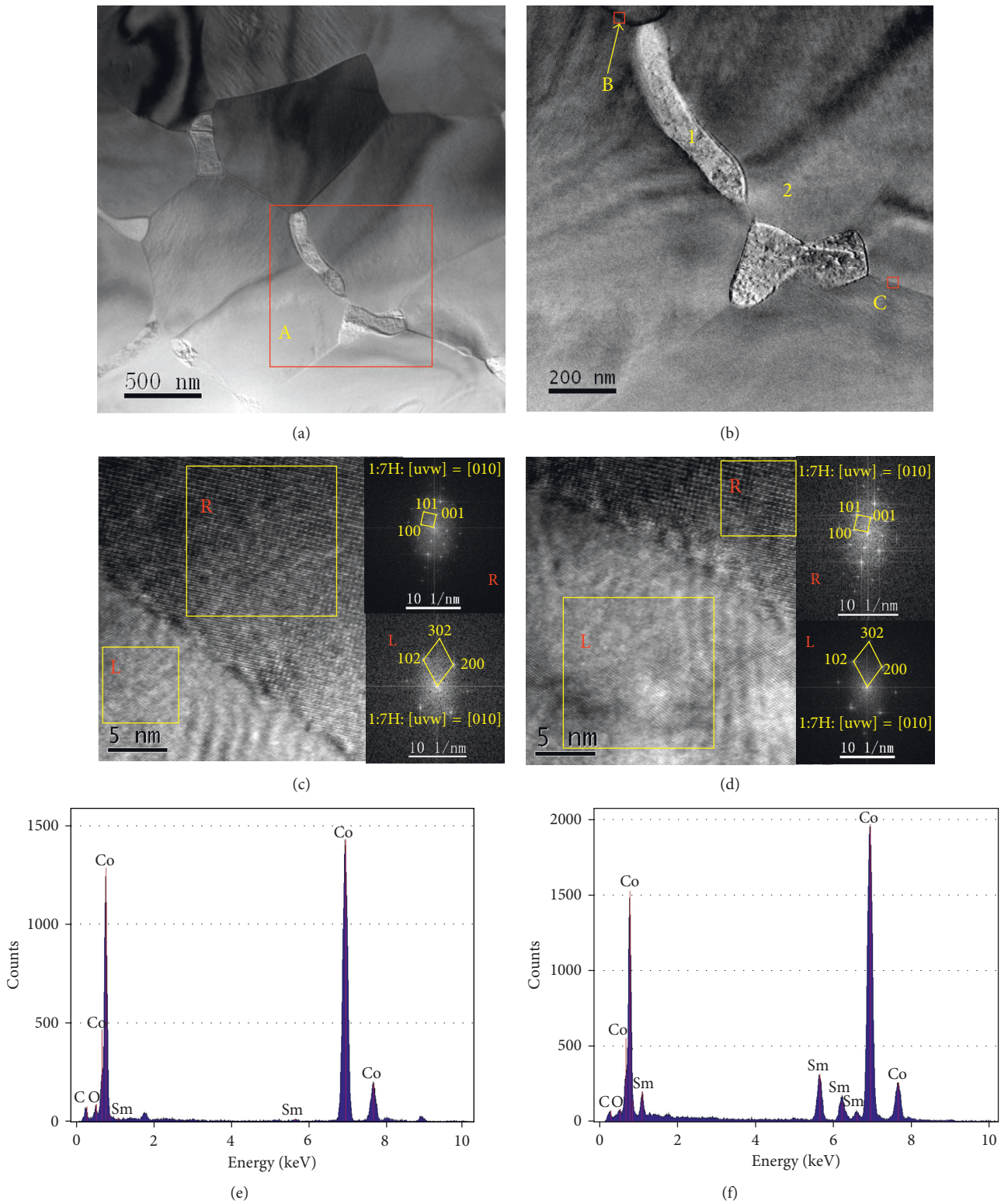


FIGURE 3: TEM images and EDS spectra of as-spun ribbons. (a) TEM image. (b) Amplified image of region A in (a). (c) Amplified image of region B in (b). (d) Amplified image of region C in (b). (e) Energy spectrum of Position 1 in (b). (f) Energy spectrum of Position 2 in (b).

the averaged long-range-ordered structural information. In contrast, EXAFS gives the information of local structure and probes the atomic environment around the interested atom [14]. Therefore, each method can contribute its own share of important information on the structure. In this work, the EXAFS method was used to analyze the slight difference of atomic structure among the three states of $SmCo_{10}$ alloy.

Considering the electronic multiscattering, atomic disorder, many-body effect, and so on, the EXAFS [14–18] function can be generally expressed as

$$\chi(k) = \sum_i N_i S_0^2 \left(\frac{f_i(k)}{kR_i^2}\right) \exp\left(-2k^2\sigma_i^2\right) \exp\left(\frac{-2R_i}{\lambda(k)}\right) \times \sin\left[2kR_i + \delta_i(k)\right], \quad (1)$$

where $i$ refers to shell of similar atoms; $k$ refers to the wave vector of photoelectrons; $\lambda(k)$ is the mean free path of the excited photoelectron; $S_0^2$ is the amplitude reduction factor of absorbing atom; $R_i$ is the distance from absorbing atom to the neighboring atoms of interest for single-scattering paths and the half-path length for multiple-scattering paths; $\sigma_i^2$ is the Debye-Waller factor (i.e., disorder factor) or the mean-square deviation versus $R_i$; $N_i$ refers to the number of atoms in the $i$th coordination shell of absorbing atom or the degeneracy for scattering paths; and $f_i(k)$ and $\delta_i(k)$ are the theoretical curved-wave amplitude and phase-shift functions of the scattering atom, respectively.

The $\lambda(k)$, $f_i(k)$, and $\delta_i(k)$ can be derived from the standard 2:17R (corresponding to Crystal Information File (CIF): 420005 in Inorganic Crystal Structure Database (ICSD)) and 1:7H (ICSD CIF: 102668) structures by FEFF [19], in which Sm is set as the center atom and $S_0^2$ and $\sigma^2$ are fixed as 1 and 0.003, respectively, and $N$ and $R$ of atomic shells with a distance of less than 6 Å from Sm are defaulted to the values calculated from the fractional coordinates of Sm and Co in standard 2:17R and 1:7H unit cells (recorded in their CIFs). Therefore, the actual structural parameters needed to be fitted in (1) are only $N_i$, $S_0^2$, $\sigma_i^2$, and $R_i$. However, different coordination shells of the absorbing atom and different scattering paths in the same shell may have different structural parameters because of some factors such as scattering atomic species, neighboring atomic environments, and vacancies. Four parameters must be fitted in each scattering path, causing difficulties in parameterization when a multishell approach is performed. Actually, too many structural parameters will result in an inaccurate and unstable result and even make the fitting process unable to be completed [20]. Therefore, it is very important to build up appropriate crystal models and use reasonable surmises and parameter associations for improving the fitting accuracy [21, 22].

First, $k$-weight Sm $L_3$-edge EXAFS ($k\chi(k)$) (as shown in Figures 4(a1)–4(a3)) was extracted from the original absorption spectra of $SmCo_{10}$ alloys at different states by Athena software package [23]. Figures 4(a1)–4(a3) show that the amplitude and oscillation frequency of $k\chi(k)$ in as-cast and annealed alloys are similar, and no obvious phase difference exists between them. However, for as-spun ribbons, the shape of $k\chi(k)$ is slightly different, and especially the amplitude is lower than that for as-cast and annealed alloys. As known from the above XRD and TEM analysis, both as-cast and annealed alloys consist of 2:17R and α-Co, and as-spun ribbons are composed of 1:7H and α-Co. The Co phase cannot contribute to the EXAFS signal because of no Sm inside, and thus $k\chi(k)$ reflects only the structural information of 2:17R or 1:7H. Therefore, we conclude that the atomic structures of the 2:17R phase in as-cast and annealed alloys are basically same but they are different from the 1:7H phase in as-spun ribbons. Especially, the 1:7H has a higher structural disorder compared with 2:17R.

In order to separate the contribution of each coordination shell of the absorbing atom from the sum of the contributions of different shells as in (1), $k\chi(k)$ was Fourier transformed without phase-shift correction by using a Hanning window with the $k$-range of 3.2–10 $Å^{-1}$ for as-cast and annealed alloys and 2.2–7.5 $Å^{-1}$ for as-spun ribbons. The smaller $k_{max}$ (7.5 $Å^{-1}$) of the $k$-range for as-spun ribbons than that (10 $Å^{-1}$) for as-cast and annealed alloys is because of the low signal-to-noise ratio (SNR) at further $k$ of greater than 7.5 $Å^{-1}$ as shown in Figure 4(a3).

Figures 4(b1)–4(b3) give the Fourier-transformed $k\chi(k)$ (FT-$k\chi(k)$) functions. Each peak in every FT-$k\chi(k)$ is related to one coordination shell, where the number of neighbors accompanied by their order degree determines the amplitude of this peak, while the position of this peak corresponds to the distance from the absorbing atom [24]. However, compared to the actual interatomic distance, the peak position will shift approximately 0.2–0.5 Å shorter because no phase-shift correction is considered for Fourier transformation [25, 26]. It can be seen that the FT-$k\chi(k)$ functions have the highest peaks in almost the same $R$-range of 1.5–3.5 Å, which illustrates that Co at this $R$-range gives main contribution on the EXAFS signal; in other words, the shape and position of the highest peak is significantly sensitive to the structural change. For the purpose of getting the subtle difference between the atomic structures of three alloys, the $R$-range of 1.5–3.5 Å for the FT-$k\chi(k)$ should be fitted by single-scattering approximation [27]. For this, the standard 2:17R structure (shown in Figure 5(a)) was used as the initial model for as-cast and annealed alloys and standard 1:7H structure (shown in Figure 5(b)) for as-spun ribbons. The two standard structures are drawn according to their CIFs. It should be noted that Figure 5(b) just shows the averaged effect of atomic positions, the actual occupancy rates of Sm and Co at 1a and 2e sites ($f_{Sm(1a)}$ and $f_{Co(2e)}$ for short) are 2/3 and 1/3, respectively. And when 1a sites are occupied by Sm, the neighboring 2e sites will never be occupied by Co [28]. That is to say, 1:7H is a disordered structure, in which some 1a and 2e sites are unoccupied.

The detailed atomic arrangement characteristics around Sm(6c) and Sm(1a) in standard 2:17R and 1:7H structures are summarized in Table 1. Considering the peak position shift, as well as combining the fitted $R$-range with Table 1, we chose these single-scattering paths of Sm(6c)-Co(18f), Sm(6c)-Co(6c), and Sm(6c)-Co(18h) to represent the structure of the 2:17R phase, and of Sm(1a)-Co(2c), Sm(1a)-Co(2e), and Sm(1a)-Co(3g) to represent the structure of the 1:7H phase, respectively. In fitting process, for reducing the structural parameters that need to be fitted, we assumed that the $N$ for each selected path is equal to the one of the corresponding path for standard structures as shown in Table 1. The Sm(6c)-Co(18f) and Sm(6c)-Co(6c) paths are merged (their $N$ is added together) as the first Co shell of Sm due to their approximate $R$ (Table 1), while Sm(6c)-Co(18h) represents the second Co shell of Sm for 2:17R. And for 1:7H,

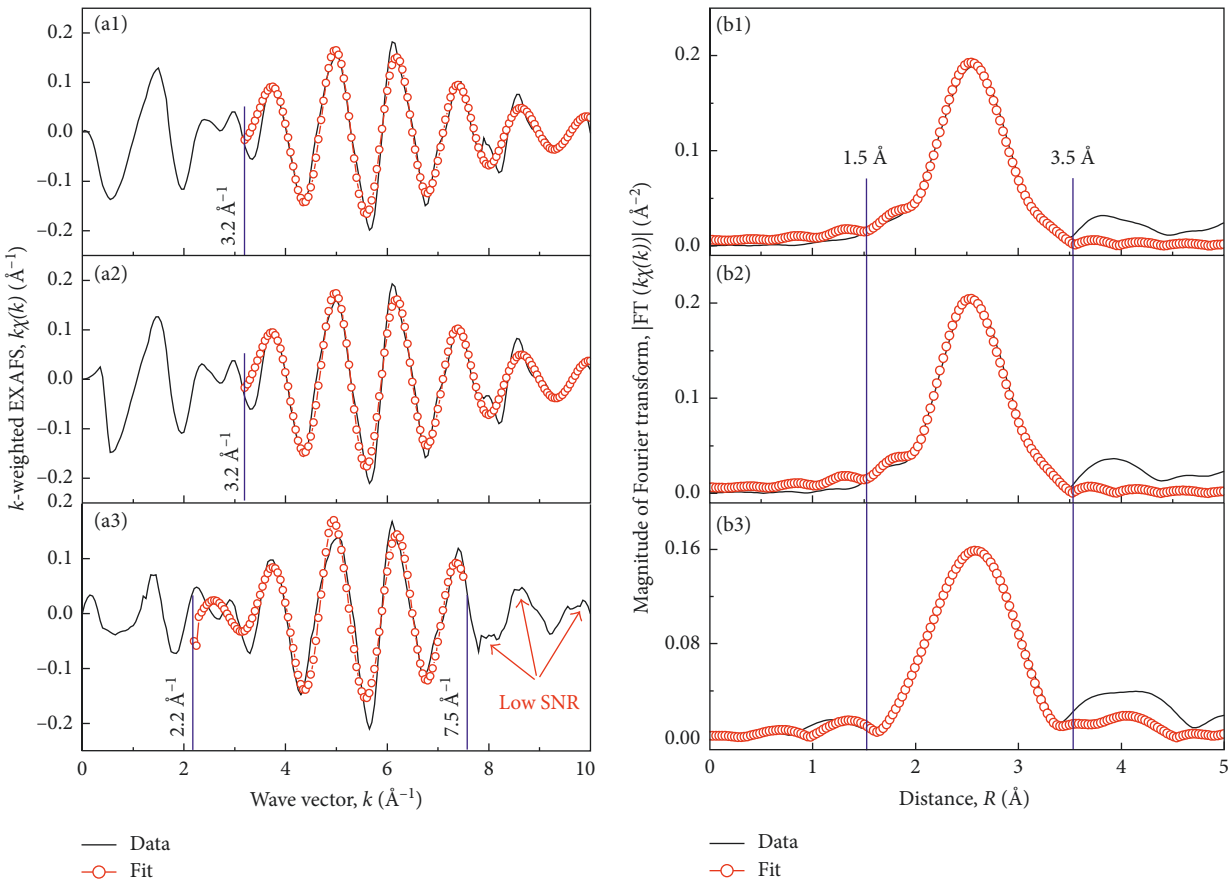


FIGURE 4: $k\chi(k)$ functions (a1–a3) and FT-$k\chi(k)$ functions (b1–b3) of $SmCo_{10}$ alloys with different states. (a1, b1) As-cast alloy. (a2, b2) Annealed alloy. (a3, b3) As-spun ribbons.

Sm(1a)-Co(2c) and Sm(1a)-Co(2e) are merged (their $N$ is added together) as the first Co shell, while Sm(1a)-Co(3g) is regarded as the second Co shell of Sm. The $R$ for the first Co shell of Sm in standard 2:17R is estimated to be 2.812 Å ($(2.801\times6+2.877\times1)/7$) according to $R$ and $N$ of Sm(6c)-Co (18f) and Sm(6c)-Co(6c) paths, while that in standard 1:7H is estimated to be 2.811 Å ($(2.804\times6+2.873\times0.667)/6.667$) according to $R$ and $N$ of Sm(1a)-Co(2c) and Sm(1a)-Co(2e) paths, as shown in Table 1. The two-shell model is necessary because the peak at $R$-range of 1.5–3.5 Å contains the contributions of two Co shells with a relatively large difference in $R$. If the two Co shells are forced to merge into one Co shell, an unreasonable result will be obtained. Moreover, the $S_0^2$ was set to 0.92 by multiple attempts using Artemis software package [23] to remove the correlation between $S_0^2$ and $\sigma^2$ due to the fact that $S_0^2$ is related to only the absorbing atomic species. The fitting results in $k$ and $R$ spaces are shown in Figure 4.

Table 2 gives the detailed fitting results with errors. The errors mainly arise from the contribution of inherent systematic deviation; moreover, the presence of a few non-smooth regions in $k\chi(k)$ also contributes to the errors. For the 2:17R phase in the annealed alloy, the $R$ of the first and second Co shells of Sm is almost the same, while $\sigma^2$ of both shells is smaller, compared to those in the as-cast alloy. It means that the 2:17R phase in as-cast and annealed alloys has the same atomic structure, but the 2:17R phase in the as-cast alloy has a higher structural disorder because the nonequilibrium crystallization caused by rapid water-cooled solidification results in an accumulation of internal stress. The annealing does not change the atomic arrangement of 2:17R but only reduces the structural disorder of 2:17R due to the relaxation of internal stress and homogenization of the microstructure by the atomic rediffusion at 820°C. Moreover, compared with the standard 2:17R structure, $\Delta R$ is both positive and negative, meaning the solid solution of Co induces the asymmetric distortion of the 2:17R structures in as-cast and annealed alloys, and the annealing at 820°C for 120 min is not enough to make the 2:17R phase reach the standard equilibrium structure. After the as-cast alloy was melt-spun, according to XRD and TEM results, the 2:17R disappeared and the metastable 1:7H was formed in the ribbons. We can see from Table 2 that $\Delta R$ for both the first and second Co shells of Sm in 1:7H is positive, and the average $\Delta R$ for 1:7H is larger than that for 2:17R, which means that the solid solubility of Co in 1:7H is higher than 2:17R. The over-dissolved Co results in a great atomic off-centered shift and asymmetric volume expansion, so a larger

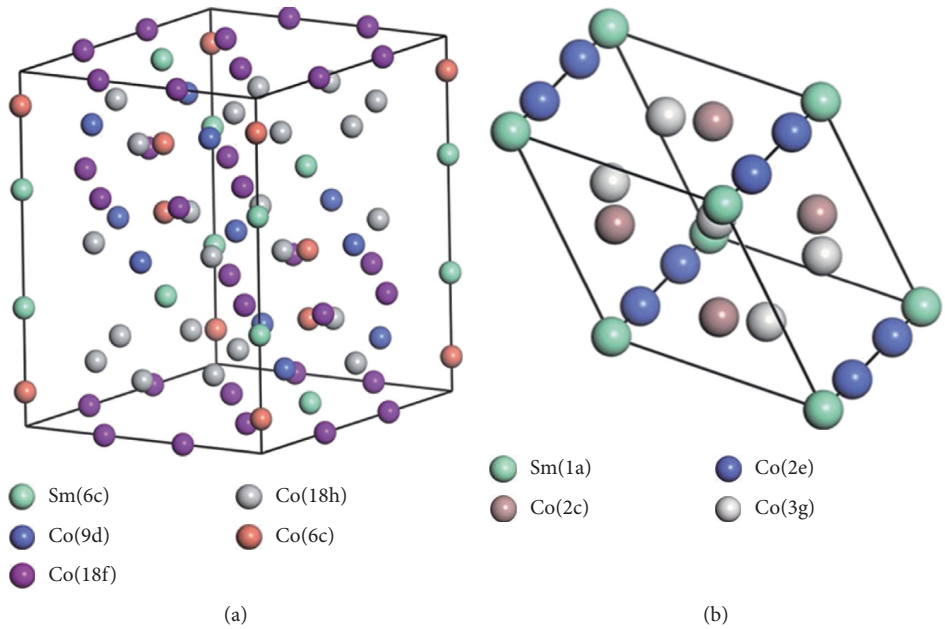


Figure 5: The standard atomic structures of 2:17R (a) and 1:7H (b). Co(6c), Co(18f), and Co(18h) represent Co at 6c, 18f, and 18h sites in 2:17R; similarly, the Co(2e), Co(2c), and Co(3g) represent Co at 2e, 2c, and 3g sites in 1:7H.

Table 1: The neighboring atomic arrangements around Sm(6c) and Sm(1a) in standard 2:17R and 1:7H structures, respectively.

| Phase | Path | Interatomic distance, $R$ (Å) | Neighboring atom number, $N$ |
|---|---|---|---|
| 2:17R | Sm(6c)-Co(18f) | 2.801 | 6 |
| | Sm(6c)-Co(6c) | 2.877 | 1 |
| | Sm(6c)-Co(18h) | 3.162 | 12 |
| | Sm(6c)-Sm(6c) | 4.057 | 1 |
| 1:7H | Sm(1a)-Co(2c) | 2.804 | 6 |
| | Sm(1a)-Co(2e) | 2.873 | 0.667 ($2f_{Co(2e)}$) |
| | Sm(1a)-Co(3g) | 3.172 | 12 |
| | Sm(1a)-Sm(1a) | 4.081 | 1.333 ($2f_{Sm(1a)}$) |

internal stress should be accumulated in 1:7H. As a result, a lower content of pure α-Co in as-spun ribbons is remained compared to that in as-cast and annealed alloys, which is consistent with the results obtained from 3.1 to 3.2 Sections. Additionally, the $\sigma^2$ of the first and second Co shells of Sm in the 1:7H phase is larger than that in the 2:17R phase in the as-cast alloy. This can be attributed to the greater internal stress and severer lattice distortion caused by more supersaturated solid solution of Co atoms in 1:7H after melt-spinning.

*3.4. VSM Analysis.* Figure 6 shows the hysteresis loops of $SmCo_{10}$ alloys and their magnetic parameters shown in the inserted table. The coercivity ($H_c$), remanence ($M_r$), and maximum magnetization at 2 T ($M_{2T}$) of as-cast and annealed alloys are 349.1 Oe, 10.8 emu/g, and 79.6 emu/g and 242.0 Oe, 11.8 emu/g, and 94.6 emu/g, respectively. The poor hard magnetic properties are similar to [3], in which Song et al. found that when the $Sm_2Co_{17}$ alloy consists of a single 2:17R or 1:7H phase, whose grains are normally coarse and no second phase acts as a strong pinning center, it shows almost no $M_r$ and $H_c$. We have known that the average sizes of 2:17R grains in as-cast and annealed alloys are both more than 30 $\mu$m and the second phase of Co with a relatively large size is discontinuously distributed on the grain boundaries together with eutectic 2:17R phase. Therefore, there is no effective exchange interaction between 2:17R and Co even if they are closely adjacent in eutecticum. On the other hand, both Co and 2:17R in eutecticum are independent phases and no Co phase is embedded in the 2:17R phase, so Co cannot act as the pinning center of 2:17R domain walls. On the contrary, the Co phase with a soft magnetism will be first reverse magnetized, ultimately making the adjacent 2:17R more easily demagnetized during demagnetization process, and thus the low $H_c$ is inevitable. Moreover, the annealed alloy has lower $H_c$ and better $M_{2T}$, which can be attributed to its small residual stress and disorder.

Figure 6 shows that the hysteresis loops of as-spun ribbons in two directions have different shapes and are neither saturated. We can see that the $H_c$ (636.5 Oe) and $M_{2T}$ (68.0 emu/g) of as-spun ribbons with magnetizing direction parallel to external field direction are both greater than those ($H_c$ = 457.8 Oe and $M_{2T}$ = 61.1 emu/g) vertical to the external field direction. The different magnetic properties along two directions of ribbon are attributed to the fact that the cooling rate along the direction perpendicular to the surface of ribbon is the fastest during melt-spinning, so the columnar grains with a specific orientation will be formed in ribbons. As a result, the as-spun ribbons show the magnetic anisotropy because the arrangement of unit cells is changed by the formation of columnar grains.

In addition, the $H_c$ of ribbons in both directions are higher than those of as-cast and annealed alloys. The EXAFS result shows that the 1:7H in as-spun ribbons has large

Table 2: The fitting results for 2:17R and 1:7H phases in $SmCo_{10}$ alloys with different states. $R_0$, calculated from the fractional coordinates of Sm and Co in standard 2:17R and 1:7H unit cells represents the distance between Sm and its first and second Co shells in standard 2:17R and 1:7H structures. $R$ factor is the sum-of-squares measure of the fractional misfit. The errors of $R$, $\sigma^2$, and $R_0$ are shown behind the "±."

| Phase | Co shells of Sm | $R$ (Å) | $\sigma^2$ (Å$^2$) | $N$ | $R_0$ (Å) | $\Delta R = R - R_0$ (Å) | $R$ factor |
|---|---|---|---|---|---|---|---|
| 2:17R in as-cast alloy | First shell | 2.985 ± 0.02 | 0.0050 ± 0.002 | 7 | 2.812 | 0.173 ± 0.02 | 0.0081 |
| | Second shell | 3.117 ± 0.03 | 0.0095 ± 0.003 | 12 | 3.162 | −0.045 ± 0.03 | |
| 2:17R in annealed alloy | First shell | 2.980 ± 0.03 | 0.0034 ± 0.001 | 7 | 2.812 | 0.168 ± 0.03 | 0.0739 |
| | Second shell | 3.117 ± 0.04 | 0.0076 ± 0.002 | 12 | 3.162 | −0.045 ± 0.04 | |
| 1:7H in as-spun ribbons | First shell | 2.872 ± 0.06 | 0.0133 ± 0.004 | 6.667 | 2.811 | 0.061 ± 0.06 | 0.0024 |
| | Second shell | 3.367 ± 0.04 | 0.0102 ± 0.002 | 12 | 3.172 | 0.195 ± 0.04 | |

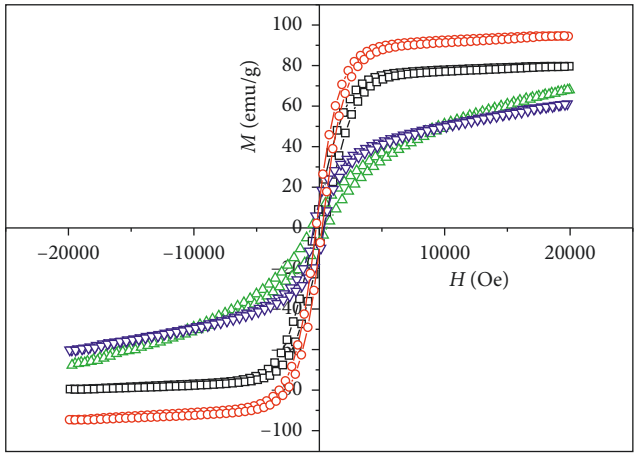


| Sample states | $H$_c (Oe) | $M$_r (emu/g) | $M$_2T (emu/g) |
|---|---|---|---|
| As-cast alloy | 349.1 | 10.8 | 79.6 |
| Annealed alloy | 242.0 | 11.8 | 94.6 |
| As-spun ribbons, parallel | 636.5 | 7.6 | 68.0 |
| As-spun ribbons, vertical | 457.8 | 13.1 | 61.1 |

As-cast alloy
Annealed alloy
As-spun ribbons, parallel
As-spun ribbons, vertical

Figure 6: Hysteresis loops of $SmCo_{10}$ alloys at different states.

average $\sigma^2$ and $\Delta R$, illustrating that it has a large residual stress arising from supersaturated solid solution of Co and asymmetry volume expansion and a high disorder of atomic arrangement. So it is the large residual stress that leads to high $H_c$ and the high structural disorder that results in low magnetization. Moreover, the short rod-shaped Co grains at grain boundaries have a large average length of ~400 nm and width of ~100 nm; the large size makes them much easier to be the nucleation sites of the reverse magnetic domains. Finally, the ribbons also exhibit small $H_c$.

Chen et al. [11] have reported that the $SmCo_{10}$ alloy prepared by ball milling $SmCo_5$ and Co powder followed by annealing exhibits the magnetic properties of $M_r = 9.4$ kG ≈ 88.0 emu/g and $H_c = 4.0$ kOe, which are better than those in Figure 6. This ascribes to a stronger exchange interaction between neighboring $Sm_2Co_{17}$ and Co grains with a smaller size of tens of nanometers. However, the $H_c$ of 4.0 kOe is also lower for practical application. Thus, we conclude that pure Sm-Co alloys with high Co content are hard to obtain excellent hard magnetic properties no matter whether the preparation method is casting, casting followed by annealing, melt-spinning, or even mechanical alloying. Trying to fine the grains of the main phase and create a thin grain boundary phase as the forceful pinning center may get more success.

## 4. Conclusion

In this paper, phase compositions, microstructures, and magnetic properties of $SmCo_{10}$ alloys prepared by three methods were studied, and the main conclusions can be drawn as follows:

(1) The as-cast $SmCo_{10}$ alloy is composed of the 2:17R matrix phase with an average grain size of ~45 $\mu$m and 2:17R + α-Co eutecticum on the grain boundaries, and the mass percentages of 2:17R and α-Co phases are ~89.4 wt% and ~10.6 wt%, respectively. The 2:17R lattice shows a little expansion due to the trace over-dissolved Co.

(2) After the as-cast alloy was annealed at 820°C for 120 min, the phase composition, phase content, and phase distribution are all unchanged. However, the average grain size of 2:17R decreases to ~35 $\mu$m, and the distribution of 2:17R + α-Co eutecticum on 2:17R matrix becomes more homogeneous. Moreover, the atomic structure of 2:17R is unchanged but with a decrease in structural disorder, and the over-dissolved Co is still remained inside after annealing. In this case, the annealed $SmCo_{10}$ alloy shows lower $H_c$ and higher $M_r$ and $M_{2T}$ than the as-cast one.

(3) After the as-cast alloy was melt-spun at 40 m/s, the 1:7H forms instead of 2:17R, and more Co is over-dissolved in 1:7H; thus, the mass percentage of α-Co in ribbons is reduced to ~4.6 wt%. The α-Co phase with the average length and width of ~400 nm and ~100 nm is distributed intermittently at the grain boundaries of the 1:7H matrix phase. Moreover, the supersaturated 1:7H shows a larger lattice expansion and higher structural disorder than 2:17R; thus, a larger internal stress is accumulated in 1:7H. As a result, the as-spun ribbons show higher $H_c$ and lower $M_{2T}$ than the as-cast and annealed alloys.

## Conflicts of Interest

The authors declare that they have no conflicts of interest.

## Acknowledgments

This work was supported by General Program from the National Natural Science Foundation of China (nos. 51671078, 51271072), National Science Fund for Young (no. 51301056), and Hebei Natural Science Foundation of China (no. E2015202008).

## Supplementary Materials

The supplementary material file named "Highlights and Graphical Abstract" contains two sections. The first section shows the highlights of this paper. The second one shows the graphical abstract, which is used to vividly describe the core of this paper. *(Supplementary Materials)*

## References

[1] J. M. D. Coey, "Permanent magnet applications," *Journal of Magnetism and Magnetic Materials*, vol. 248, no. 3, pp. 441–456, 2002.

[2] X. Su, W. Zhang, G. Liu, and Z. Du, "A thermodynamic assessment of the Co-Sm system," *Journal of Alloys and Compounds*, vol. 267, no. 1-2, pp. 149–153, 1998.

[3] X. Song, N. Lu, M. Seyring et al., "Abnormal crystal structure stability of nanocrystalline $Sm_2Co_{17}$ permanent magnet," *Applied Physics Letters*, vol. 94, no. 2, p. 023102, 2009.

[4] A. E. Ray, "Metallurgical behavior of $Sm(Co,Fe,Cu,Zr)_z$ alloys," *Journal of Applied Physics*, vol. 55, no. 6, pp. 2094–2096, 1984.

[5] X. Y. Xiong, T. Ohkubo, T. Koyama, K. Ohashi, Y. Tawara, and K. Hono, "The microstructure of sintered Sm $(Co_{0.72}Fe_{0.20}Cu_{0.055}Zr_{0.025})_{7.5}$ permanent magnet studied by atom probe," *Acta Materialia*, vol. 52, no. 3, pp. 737–748, 2004.

[6] K. D. Durst, H. Kronmüller, and W. Ervens, "Investigations of the magnetic properties and demagnetization processes of an extremely high coercive $Sm(Co,Cu,Fe,Zr)_{7.6}$ permanent magnet II. The coercivity mechanism," *physica Status Solidi (a)*, vol. 108, no. 2, pp. 705–719, 1988.

[7] J. C. Tellez-Blanco, X. C. Kou, R. Grössinger, E. Estevez-Rams, J. Fidler, and B. M. Ma, "Coercivity and magnetic anisotropy of sintered $Sm_2Co_{17}$-type permanent magnets," *Journal of Applied Physics*, vol. 82, no. 8, pp. 3928–3933, 1997.

[8] A. Yan, A. Bollero, K. H. Müller, and O. Gutfleisch, "Influence of Fe, Zr, and Cu on the microstructure and crystallographic texture of melt-spun 2:17 Sm–Co ribbons," *Journal of Applied Physics*, vol. 91, no. 10, pp. 8825–8827, 2002.

[9] A. Yan, O. Gutfleisch, A. Handstein, T. Gemming, and K. H. Müller, "Microstructure, microchemistry, and magnetic properties of melt-spun $Sm(Co,Fe,Cu,Zr)_z$ magnets," *Journal of Applied Physics*, vol. 93, no. 10, pp. 7975–7977, 2003.

[10] O. Gutfleisch, K. H. Müller, K. Khlopkov et al., "Evolution of magnetic domain structures and coercivity in high-performance SmCo 2:17-type permanent magnets," *Acta Materialia*, vol. 54, no. 4, pp. 997–1008, 2006.

[11] S. K. Chen, J. L. Tsai, and T. S. Chin, "Nanocomposite $Sm_2Co_{17}$/Co permanent magnets by mechanical alloying," *Journal of Applied Physics*, vol. 79, no. 8, pp. 5964–5966, 1996.

[12] Y. Yuan, J. Yi, G. Borzone, and A. Watson, "Thermodynamic modeling of the Co-Sm system," *Calphad*, vol. 35, no. 3, pp. 416–420, 2011.

[13] H. M. Rietveld, "A profile refinement method for nuclear and magnetic structures," *Journal of Applied Crystallography*, vol. 2, no. 2, pp. 65–71, 1969.

[14] S. J. Gurman, N. Binsted, and I. Ross, "A rapid, exact curved-wave theory for EXAFS calculations," *Journal of Physics C: Solid State Physics*, vol. 17, no. 1, pp. 143–151, 1984.

[15] J. J. Rehr and R. C. Albers, "Theoretical approaches to x-ray absorption fine structure," *Reviews of Modern Physics*, vol. 72, no. 3, pp. 621–654, 2000.

[16] E. A. Stern, "Structure determination by X-ray absorption," *Contemporary Physics*, vol. 19, no. 4, pp. 289–310, 1978.

[17] Z. Sun, Q. Liu, T. Yao, W. Yan, and S. Wei, "X-ray absorption fine structure spectroscopy in nanomaterials," *Science China Materials*, vol. 58, no. 4, pp. 313–341, 2015.

[18] N. A. Young, "The application of synchrotron radiation and in particular X-ray absorption spectroscopy to matrix isolated species," *Coordination Chemistry Reviews*, vol. 277-278, pp. 224–274, 2014.

[19] J. J. Rehr, J. Mustre de Leon, S. I. Zabinsky, and R. C. Albers, "Theoretical X-ray absorption fine structure standards," *Journal of the American chemical society*, vol. 113, no. 14, pp. 5135–5140, 1991.

[20] E. A. Stern, "Number of relevant independent points in x-ray-absorption fine-structure spectra," *Physical Review B*, vol. 48, no. 13, pp. 9825–9827, 1993.

[21] S. C. Siah, R. Jaramillo, R. Chakraborty et al., "X-ray absorption spectroscopy study of structure and stability of disordered $(Cu_2SnS_3)_{1-x}(ZnS)_x$ alloys," *IEEE Journal of Photovoltaics*, vol. 5, no. 1, pp. 372–377, 2015.

[22] K. Provost, E. C. Beret, D. Muller, E. S. Marcos, and A. Michalowicz, "Impact of the number of fitted Debye-Waller factors on EXAFS fitting," *Journal of Physics: Conference Series*, vol. 430, no. 1, p. 012015, 2013.

[23] B. Ravel and M. Newville, "ATHENA and ARTEMIS: interactive graphical data analysis using IFEFFIT," *Physica Scripta*, vol. 115, pp. 1007–1010, 2005.

[24] I. L. Graff, S. R. Teixeira, L. Amaral, M. M. Alves, and W. H. Flores, "Structural modifications in $Fe_xCo_{1-x}$/Cu multilayers induced by ion irradiation," *Journal of Applied Physics*, vol. 96, no. 3, pp. 1469–1474, 2004.

[25] D. C. Koningsberger, B. L. Mojet, G. E. van Dorssen, and D. E. Ramaker, "XAFS spectroscopy; fundamental principles and data analysis," *Topics in Catalysis*, vol. 10, no. 3-4, pp. 143–155, 2000.

[26] T. Tangcharoen, C. Kongmark, and W. Pecharapa, "Synchrotron X-ray absorption spectroscopy study of the local atomic structures and cation ordering in perovskite- and spinel-type zinc stannate synthesized by co-precipitation method," *Journal of Molecular Structure*, vol. 1102, pp. 95–100, 2015.

[27] V. L. Aksenov, M. V. Koval'chuk, A. Y. Kuz'min, Y. Purans, and S. I. Tyutyunnikov, "Development of methods of EXAFS spectroscopy on synchrotron radiation beams," *Crystallography Reports*, vol. 51, no. 6, pp. 908–935, 2006.

[28] Y. Khan, "On the crystal structures of the $R_2Co_{17}$ intermetallic compounds," *Acta Crystallographica Section B: Structural Crystallography and Crystal Chemistry*, vol. 29, no. 11, pp. 2502–2507, 1973.